INSTITUTE OF PHYSICS PUBLISHING and INTERNATIONAL ATOMIC ENERGY AGENCY NUCLEAR FUSION

Nucl. Fusion **43** (2003) 1031–1039 PII: S0029-5515(03)67186-3

Modelling of ELM-like phenomena via mixed SOC-diffusive dynamics

R. Sánchez[1,a], D.E. Newman[2], B.A. Carreras[3], R. Woodard[2], W. Ferenbaugh[2] and H.R. Hicks[3]

[1] Universidad Carlos III de Madrid, 28911 Leganés, Madrid, Spain
[2] University of Alaska-Fairbanks, Fairbanks, AK 99775-5920, USA
[3] Oak Ridge National Laboratory, Oak Ridge, TN 37831-8070, USA

E-mail: rsanchez@fis.uc3m.es

Received 14 October 2002, accepted for publication 4 August 2003
Published 4 September 2003
Online at stacks.iop.org/NF/43/1031

Abstract
A sandpile model describing some of the features of plasma turbulent transport dynamics in the L-mode is extended, by adding appropriate new dynamics, to exhibit a transition to enhanced confinement modes. As a result, H-modes with and without edge localized modes (ELMs) can both be obtained by varying the appropriate parameters. Each exhibits features reminiscent of what is observed in confined plasmas. The interplay between an avalanche and a diffusive transport mechanism is shown to be essential, in this context, for the system to display periodic edge ELMing.

PACS numbers: 52.55.Dy, 52.55.Fa, 52.35.Ra, 05.45.−a, 05.65.+b

1. Introduction

A few years ago, self-organized criticality [1] (SOC) was proposed as a possible paradigm for plasma turbulent transport dynamics in fusion devices [2, 3]. SOC systems have the ability to organize themselves and to fluctuate around a state marginal to a major disruption, exhibiting scale-free transport. The key ingredient for the appearance of SOC is the existence of two disparate timescales, respectively associated with the drive and with the instability relaxation. Since this condition is usually fulfilled in systems with instability thresholds, it was proposed that SOC might apply to a plasma confined in the L-mode [3]. The idea of the plasma staying in a SOC-like state is attractive, since it can help in understanding several experimental results encountered in the L-mode [4], such as the non-gyro-Bohm scaling of the confinement time, the existence of canonical profiles, the observation of power degradation and the superdiffusive propagation of cold and heat pulses [5]. Some experimental evidence consistent with this idea has already been reported. It claims self-similarity for electrostatic edge fluctuations [6, 7], the existence of long-range temporal correlations in them [8, 9] and the observation of radial propagation of avalanche-like events in L-mode discharges [10].

The existence of an H-mode confinement state and its transition from the L-mode opens a new challenge to the SOC transport paradigm. Quasi-periodic oscillations have been observed before in SOC systems, but their relevance to the H-mode is still unclear. For instance, we introduced a diffusive sandpile in [11], in which global oscillations come to dominate the dynamics after the diffusivity becomes sufficiently large to compete with avalanche transport efficiently in setting the profile roughness. Even when this could be achieved for fairly small diffusivities, the efficiency of this process improves in the opposite direction (in parameter space) to that in which edge localized modes (ELMs) are observed (in tokamaks, ELMs are observed when the external power increases, which would reduce the efficiency of diffusivity to carry out this task). On the other hand, Chapman *et al* [12] obtained global quasi-periodic oscillations with different sandpile dynamics by varying a characteristic scale for energy-redistribution, but it is not clear how changes in this parameter might correlate to changes in the external drive. Finally, in [13], Hicks *et al* also observe quasi-periodic behaviour when avalanche events are temporally trapped inside a transport barrier, which gives to these events a more transient character than observed in experiments. The basic difficulty in bringing all these models closer to a confined plasma is the limited dynamics they can exhibit as a result of the small number of parameters that define them. This fact gives them a strong universal character (in the sense that the behaviour observed is rather insensitive to the details of the system), but it also reduces the wealth of behaviour that can be observed. For this reason, in this paper, we explore whether a sandpile model for the L-mode can be extended to exhibit a transition into

[a] Author to whom any correspondence should be addressed.

the H-mode and to produce ELMs, by adding new dynamics inspired in what are thought to be the responsible physical mechanisms. We acknowledge that this approach somewhat reduces the universality of the model but, by adding a handful of free parameters appropriately, this extended model provides us with a highly simplified system in which the interaction of these mechanisms could be isolated and studied, helping to shed some light on the relevance (if any) of SOC in this context.

The paper is then organized as follows: in section 2, the diffusive sandpile is introduced as a simple model that captures the basic physics of L-mode dynamics. Then, in section 3, this sandpile is extended by adding a few new rules and parameters. All of them are inspired by the physical mechanisms that are thought to be responsible for the L–H transition in a real confined plasma [14, 15]. It is shown that, for appropriate values of the new free parameters, the sandpile rules make it possible that both ELM-free and Type-I ELMy H-modes be accessed as the external power increases. In section 4, the confinement time of the sandpile in all these regimes is estimated both analytically and numerically. The obtained scalings prove the enhanced-confinement character of the so-called sandpile H-modes. In section 5, the Type-I ELMs observed at the highest powers are characterized and the dependence on the total external power of their frequency and sizes, as well as some other of their temporal and dynamical features, are studied. Finally, some conclusions are drawn in section 6.

2. The diffusive sandpile: a model for L-mode dynamics

We use a running diffusive sandpile [6] as the simplest model that captures the essential dynamical features of plasma transport in the L-mode (see figure 1). The sandpile consists of L cells, each labelled by an index $n \in [1, L]$. Each cell stores an amount of sand h_n. U_0 grains of sand are dropped randomly on every cell at each iteration with probability P_0. The external drive per cell is thus $S_0 = U_0 P_0$. SOC dynamics

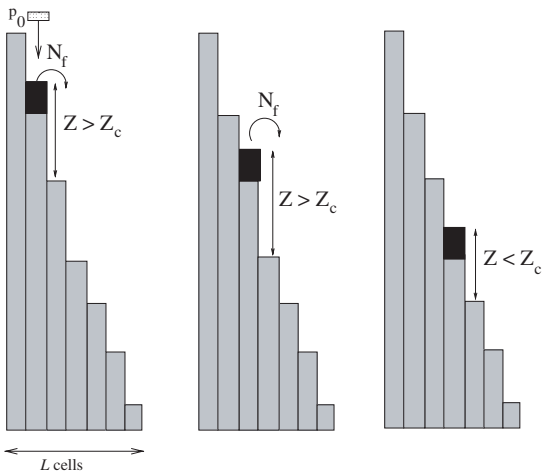

Figure 1. Diagram explaining the diffusive sandpile rules. First, sand is added randomly to every cell. Then, cells are checked for stability and, if unstable, N_F grains of sand are moved to the next cell. Finally, at each iteration, a diffusive net flux is added (or subtracted if negative) to each cell.

appear because of the existence of a critical sand slope $-Z_c$ that, when locally overcome, triggers the removal of N_F grains of sand to the next cell. To this avalanche transport channel, a second channel is added. A local diffusive flux Γ is computed at each cell as $\Gamma_n = D_0(Z_{n+1} - Z_n)$, where D_0 is the diffusion coefficient and $Z_n = h_{n+1} - h_n$ is the local slope. Finally, the sandpile has an open boundary at $n = L$, from which sand is removed (Notice that Z_c is chosen to be positive which implies that, throughout the paper, a cell is unstable if the local slope $Z \leqslant -Z_c$, since Z is negative due to the fact that sand leaves the sandpile at the edge.)

For $S_0 L < D_0(Z_c - N_F/2)$, the system has a diffusion dominated regime that we call the ohmic phase by analogy with tokamak confinement. In this phase, the slope profile is determined by the strength and distribution of the source. The condition on the external power is set by the maximum flux that can leave the sandpile through the diffusive channel without the edge cell becoming unstable. Since the drive we use is uniformly distributed, the typical slope profile is linear all across the sandpile (see the slope profile in full down triangles in the lower left part of figure 2). However, for $S_0 L > D_0(Z_c - N_F/2)$, the diffusive sandpile makes a transition into a different regime. The slope profile divides into two regions (see profile in open left triangles in figure 2), a diffusive core where transport is still dominated by diffusion and a SOC region (with a constant slope just above $-Z_c$), where transport is mainly driven via avalanches. The point that connects both regions can be easily estimated to be located at:

$$x_1 \simeq \frac{D_0(Z_c - N_F/2)}{S_0}. \tag{1}$$

In contrast to the ohmic phase (and to the diffusive core), the slope profile in the SOC region is independent of the distribution of the drive source. And the sandpile now has many of the dynamical characteristics of the L-mode observed in confined plasmas: transport in the SOC region is scale-free, with contributing scales only limited by the size of the SOC region (this implies a non-gyro-Bohm scaling of confinement, as will be shown in section 4); the absolute value of the slope stays on average very close to (but below) $Z_c - N_F/2$, which reminds one of the canonical profiles observed in many devices; power degradation is observed (which will be shown in section 4); and, finally, any perturbation of the slope profile can propagate superdiffusively (if $\Delta Z \gg N_F/2$) or diffusively (if $\Delta Z \ll N_F/2$). For these reasons, we will claim that this regime of the diffusive sandpile captures many of the characteristic features of the L-mode in a confined plasma, and we will accordingly call it the sandpile L-mode.

Since the relevant limit in fusion plasmas is $D_0/P_0 \ll 1$ (which implies that diffusive losses provide a small contribution to the total transport), it might seem that D_0 would never play any important role in the dynamics. Therefore, this diffusive sandpile should not add anything intrinsically new to the dynamics of the standard non-diffusive sandpile used in the past [3]. This statement is, however, not correct. In the diffusive sandpile it is possible to achieve $\kappa \equiv D_0 N_F^2/P_0 \gg 1$ while still satisfying $D_0/P_0 \ll 1$, which takes the diffusive sandpile into a new dynamical regime. κ gives a measure of the competition between the roughening of the slope profile caused by avalanches and its smoothing by diffusion. When

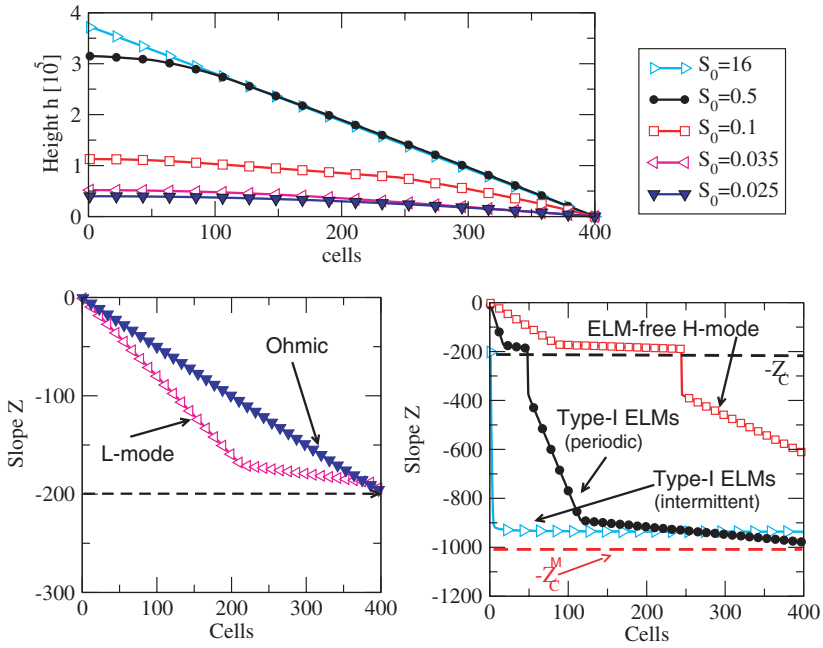

Figure 2. Height and slope profiles of the diffusive sandpile as the external power is increased, showing the path of the system across the different regimes. (Parameters: $D_0 = 0.05$; $L = 400$; $Z_c = 200$; $N_F = 30$; $Z_c^M = 1000$; $N_F^M = 120$; $k = 10$.)

the latter dominates (for $\kappa > \kappa_c$, with the critical value given approximately by $\kappa_c \simeq 20$ [16]), diffusion is not yet sufficiently important to dominate the total transport (still mainly driven through avalanches), but it can efficiently erase all inhomogeneities in the slope profile. This causes SOC to disappear. In its place, a quasi-periodic relaxation of the edge extending all across the SOC region balances the external power to maintain a steady state (see figure 5 in [16]). As we will see, this transition may open a possible route to ELM-like relaxations once the diffusive sandpile has entered the H-mode.

3. Physics-based extension of the SOC-diffusive sandpile

In tokamak plasmas, H-mode is achieved when the external power exceeds the threshold value for the L–H transition [17]. A transport barrier then forms at the edge that is thought to be triggered by the sheared-flow-induced suppression of turbulence [14, 15]. After the transition, the confinement time seems to follow a gyro-Bohm scaling, at least in its ion channel [18]. Once the system is in the H-mode, several edge relaxation processes may successively appear as power increases. Type-III ELMs appear first. These are small periodic relaxations with frequency (amplitude) that decreases (increases) with the external power. As power continues to increase, Type-III ELMs give way to an ELM-free phase. Finally, at even larger powers, large Type-I ELMs appear, with a frequency that increases with power. The standard view of these phenomena relates Type-III ELMs to resistive modes, while Type-I ELMs are associated with the much faster ideal ballooning modes [19].

Several ways may be envisioned to make the sandpile undergo a transition into an H-mode. In our case, we have tried to capture the effect of the shear-induced suppression of the local transport by varying the sandpile relaxation rules that deal with overdriven cells. These overdriven cells appear as follows: as the external power increases, the flux that must leave the sandpile through its edge increases as well. Eventually, the balancing of the external power will require that the flux leaving the sandpile exceeds the maximum flux that can go through the edge cell while it stays subcritical on average (i.e. with its average slope staying above $-Z_c$). This maximum flux would be equal to $N_F/2$ in the absence of diffusive transport, which corresponds to the limit case of continuous edge relaxation. If diffusion is taken into account, the flux limit is overcome for $S_0 \geqslant S_0^{L-H}$, where $S_0^{L-H} \simeq (N_F/2 + D_0 Z_c)/L$. At higher powers, the number of overdriven cells increases, extending inwards from the sandpile edge. The new relaxation rule for any of these overdriven cells is to substitute the transfer of N_F grains to the next cell by a 'turbulent' diffusive flux, with diffusion coefficient given by $D_t = N_F/(kZ_c)$. Since this flux is added to the ambient diffusion given by D_0, the effective diffusivity at these cells is $D_e = D_0 + D_t$. Note that with this prescription, the local transport at these cells is reduced by k times (relative to that produced by the normal overlapping rule) when the slope is close to $-Z_c$. Therefore, the local slope must increase (in absolute value) to balance the external power, which causes the formation of the barrier. But at the same time, the diffusive turbulent flux brings into the dynamics the radial transport decorrelation associated with the shear-suppression mechanism, which is suspected to be responsible for the transition of the confinement time towards gyro-Bohm scaling [3].

The new relaxation rule has the effect of allowing the formation of a diffusive pedestal for $S_0 > S_0^{L-H}$ (see slope profile in open squares in figure 2). This new regime will be called the sandpile ELM-free H-mode. It will be seen later (see section 4) that in this ELM-free H-mode confinement improves and changes its scaling with the sandpile parameters. Also, no ELMing activity is observed. From a simple power

balance calculation, the location where the diffusive pedestal starts is approximately given by:

$$x_2 \simeq \frac{N_F/2 + D_0 Z_c}{S_0}. \tag{2}$$

The width of the diffusive pedestal ($\Delta_2 = L - x_2$) is therefore an increasing function of S_0, that reaches a final limit value ($\Delta_2 \simeq L$) when the total power reaches $S_0 = (N_F/2 + D_0 Z_c)$. However, a comment must be made at this point. The fact that more and more of the cells must go supercritical to balance the always increasing external drive is related to the absence of any other transport mechanism in the system. In a real plasma, the increase in width of the pedestal might be limited by the encounter with another transport mechanism as the pedestal propagates inwards (such as ion or electron temperature-gradient modes, that might dominate the core transport). These modes might take care of balancing the external drive without going supercritical. In this case, the width of the pedestal will no longer increase to cover the whole system.

The second physics-based change in the diffusive sandpile rules will open the route into an ELMy H-mode. As we commented before, Type-I ELMs are usually related to the ideal instabilities that would be triggered when the local critical gradient for these modes is overcome [19]. Therefore, we will introduce a second critical gradient $-Z_c^M \ll -Z_c$, that will trigger the transfer of $N_F^M \gg N_F$ grains of sand when any cell goes unstable. The much faster temporal scales associated with ideal MHD activity are included by relaxing these avalanches differently: instead of constraining the relaxation to affect only one cell per iteration (as is the case for cells unstable relative to Z_c), the relaxations relative to Z_c^M will be continued in the same iteration until no more free energy is available.

The existence of this second critical gradient makes the system transit into a Type-I ELMy H-mode when $S_0 > D_e(Z_c^M - N_F^M/2)/L$. A second pedestal (that we will call the *SOC pedestal*) then appears with a steeper slope (see slope profile in filled circles in figure 2), whose absolute value varies linearly between $Z_c^M - N_F^M/2$ and Z_c^M. The location where this pedestal starts is found to be at

$$x_3 \simeq \frac{D_e(Z_c^M - N_F^M/2)}{S_0}. \tag{3}$$

As in the case of the diffusive pedestal observed in ELM-free H-mode, the SOC pedestal width ($\Delta_3 = L - x_3$) is an increasing function of S_0 that saturates (at $\Delta_3 \simeq L$) for total power $S_0 \geqslant D_e(Z_c^M - N_F^M/2)$. However, the same considerations that we already made for the diffusive pedestal width must also be made regarding that of the SOC pedestal. And, in particular, the effects on the periodicity of ELMs of a possible blocking of the pedestal advance by a second transport mechanism should be considered.

As an example of the ELMing activity typical of this regime, the temporal trace of the flux leaving the sandpile for $S_0 = 0.5$ is shown in figure 3. A very clear ELM-like periodic relaxation is observed and, between ELMs, an increasing diffusive flux (see zoom of the same figure) reveals the increase of Z_{edge} towards Z_c^M in absolute value. As will be discussed in section 5, the frequency of these relaxations increases linearly with S_0. However, there is a value of the power ($S_0 \simeq D_e(N_F^M)^2/\kappa_c$) above which the relaxations transform from periodic to intermittent (see upper frame in figure 4). When this happens, the slope profile is no longer linear across the SOC pedestal, but approximately constant at $-[Z_c^M - N_F^M/2]$, as shown in figure 2 (see curve in right open triangles). Therefore, we will distinguish in what follows between periodic and intermittent Type-I ELMy H-modes.

As a final comment, we want to stress the point that the rules we have chosen to produce a sandpile H-mode are by no means unique. Any rule that guarantees the damping of avalanche formation beyond the transition point can be used to provide the same dynamical behaviour. For instance, Gruzinov *et al* [20] proposed recently an alternate prescription when exploring several issues related instead to the dynamics of pedestal formation at the L–H transition. Their rule relies on the existence of a bracket of slope values $[-Z_{c_2}, -Z_{c_1}]$ in which the sandpile is unstable. In this way, avalanches cease to be triggered when the slope locally becomes more negative than $-Z_{c_2}$, and a pedestal and an H-mode are also achieved. In contrast, the role played by the diffusivity in this context is not arbitrary, since no quasi-periodic ELMs would exist otherwise.

4. Scaling of the diffusive sandpile confinement time

Both the ELM-free H-mode and the Type-I ELMy H-modes are enhanced confinement regimes compared to the L-mode. To prove it, we define the confinement time of the sand in the diffusive sandpile as:

$$\tau_E = \frac{\int_0^L \left[\int_L^x Z(x')\,dx'\right] dx}{S_0 L}, \tag{4}$$

where the integral represents the amount of sand confined in the sandpile in a steady state, and $S_0 L$ is the total external power. τ_E is a function of the parameters that define the sandpile: D_0, D_e, L, S_0, Z_c, Z_c^M, N_F and N_F^M.

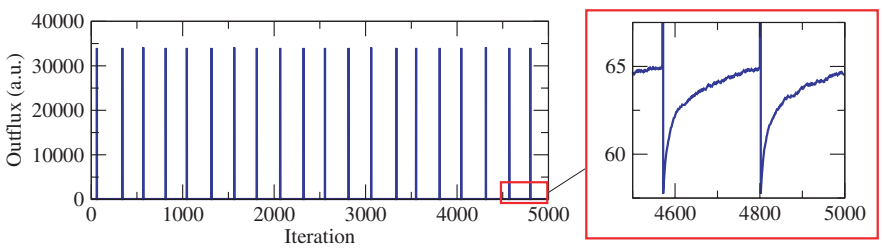

Figure 3. Time traces of the flux leaving the sandpile for $S_0 = 0.5$ in the Type-I ELMy H-mode.

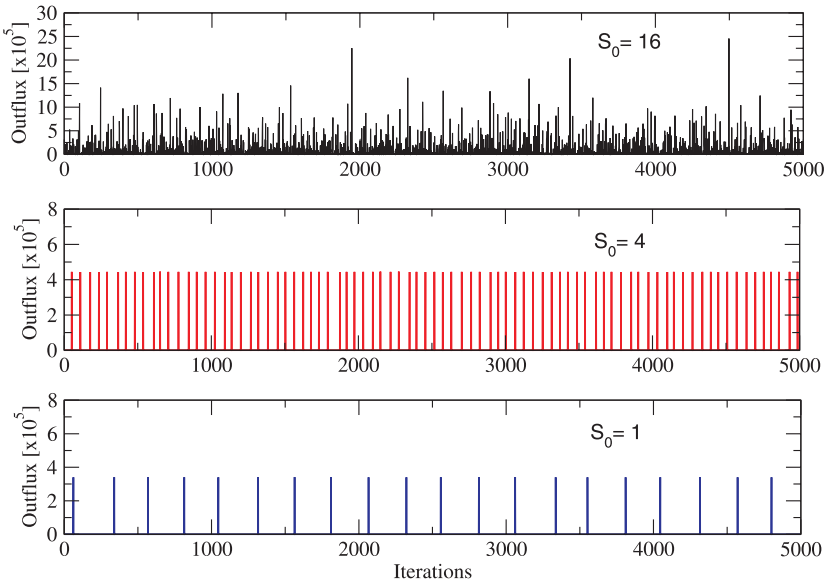

Figure 4. Time traces of the flux leaving the sandpile in the ELMy H-mode for different values of S_0.

The slope profiles can be estimated analytically in all regimes as:

- Ohmic:

$$Z(x) = -\left(\frac{S_0}{D_0}\right)x, \qquad 0 < x < L. \tag{5}$$

- L-mode:

$$Z(x) = \begin{cases} -\left(\dfrac{S_0}{D_0}\right)x, & 0 < x < x_1, \\ -\left(Z_c - \dfrac{N_F}{2}\right), & x_1 < x < L. \end{cases} \tag{6}$$

- ELM-free H-mode:

$$Z(x) = \begin{cases} -\left(\dfrac{S_0}{D_0}\right)x, & 0 < x < x_1, \\ -\left(Z_c - \dfrac{N_F}{2}\right), & x_1 < x < x_2, \\ -\left(\dfrac{S_0}{D_e}\right)x, & x_2 < x < L. \end{cases} \tag{7}$$

- Type-I ELMy H-mode (periodic):

$$Z(x) = \begin{cases} -\left(\dfrac{S_0}{D_0}\right)x, & 0 < x < x_1, \\ -\left(Z_c - \dfrac{N_F}{2}\right), & x_1 < x < x_2, \\ -\left(\dfrac{S_0}{D_e}\right)x, & x_2 < x < x_3, \\ -\left(Z_c^M - \dfrac{N_F^M}{2}\right) - \dfrac{N_F^M(x - x_3)}{2(L - x_3)}, & \\ x_3 < x < L. \end{cases} \tag{8}$$

- Type-I ELMy H-mode (intermittent):

$$Z(x) = \begin{cases} -\left(\dfrac{S_0}{D_0}\right)x, & 0 < x < x_1, \\ -\left(Z_c - \dfrac{N_F}{2}\right), & x_1 < x < x_2, \\ -\left(\dfrac{S_0}{D_e}\right)x, & x_2 < x < x_3, \\ -\left(Z_c^M - \dfrac{N_F^M}{2}\right), & x_3 < x < L. \end{cases} \tag{9}$$

Then, using equation (4), the following confinement times are obtained (the interval of external power over which each formula holds is bracketed next to the regime name):

- Ohmic [$S_0 < D_0(Z_c - N_F/2)/L$]:

$$\tau_E^{\text{Ohmic}} = \frac{L^2}{3D_0}. \tag{10}$$

- L-mode [$D_0(Z_c - N_F/2)/L < S_0 < (N_F/2 + D_0 Z_c)/L$]:

$$\tau_E^{\text{L-mode}} = \frac{(Z_c - N_F/2)L}{2S_0} - \frac{D_0^2(Z_c - N_F/2)^3}{6S_0^3 L}. \tag{11}$$

- ELM-free H-mode [$(N_F/2 + D_0 Z_c)/L < S_0 < D_e(Z_c^M - N_F^M/2)/L$]:

$$\tau_E^{\text{ELM-free H-mode}} = \frac{L^2}{3D_e} - \frac{(N_F/2 - D_0 Z_c)^2}{2S_0^3 L} \times \left[\frac{2(N_F/2 - D_0 Z_c)}{3D_e} - \left(Z_c - \frac{N_F}{2}\right)\right] - \frac{D_0^2(Z_c - N_F/2)^3}{6S_0^3 L}. \tag{12}$$

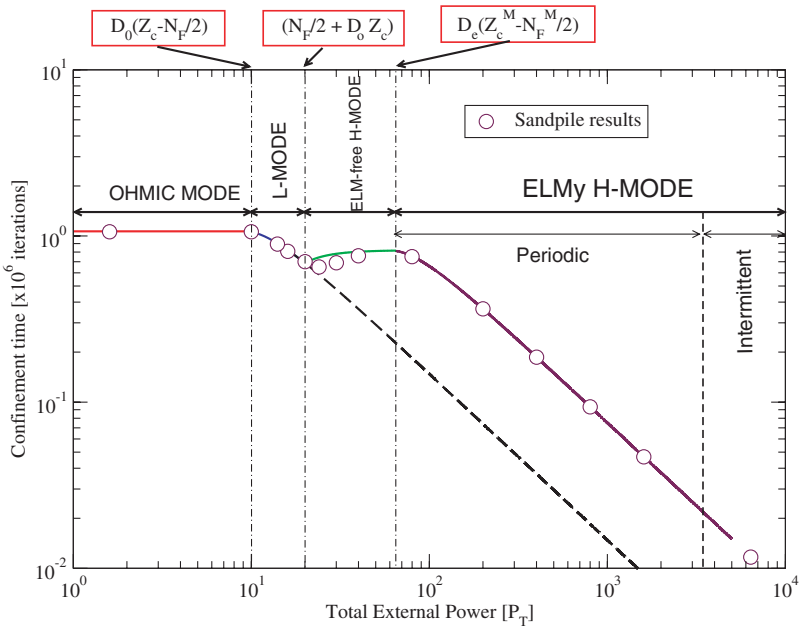

Figure 5. Comparison of the analytic formulae for τ_E with numerical calculations. The dashed line extrapolates the L-mode beyond the power threshold for the L–H transition for easier comparison.

- Type-I ELMy H-mode (periodic) $[D_e(Z_c^M - N_F^M/2)/L < S_0 < D_e(N_F^M)^2/\kappa_c]$:

$$\tau_E^{\text{ELMy H-mode (periodic)}} = \frac{(Z_c^M - N_F^M/6)L}{2S_0} - \frac{N_F D_e(Z_c^M - N_F^M/2)}{6S_0^2} - \frac{N_F D_e^2(Z_c^M - N_F^M/2)^2}{12S_0^3 L} - \frac{D_e^2(Z_c^M - N_F^M/2)^3}{6S_0^3 L} - \frac{(N_F/2 - D_0 Z_c)^2}{2S_0^3 L} \times \left[\frac{2(N_F/2 - D_0 Z_c)}{3D_e} - \left(Z_c - \frac{N_F}{2}\right)\right] - \frac{D_0^2(Z_c - N_F/2)^3}{6S_0^3 L}. \quad (13)$$

- Type-I ELMy H-mode (intermittent) $[S_0 > D_e(N_F^M)^2/\kappa_c]$:

$$\tau_E^{\text{ELMy H-mode (intermittent)}} = \frac{(Z_c^M - N_F^M/2)L}{2S_0} - \frac{D_e^2(Z_c^M - N_F^M/2)^3}{6S_0^3 L} - \frac{(N_F/2 - D_0 Z_c)^2}{2S_0^3 L} \times \left[\frac{2(N_F/2 - D_0 Z_c)}{3D_e} - \left(Z_c - \frac{N_F}{2}\right)\right] - \frac{D_0^2(Z_c - N_F/2)^3}{6S_0^3 L}. \quad (14)$$

All these expressions (equations (10)–(14)) agree very well with the results for τ_E obtained numerically (see figure 5). Several interesting conclusions can be drawn when analysing them in similar ways to those used in studies of confinement of fusion plasmas [18, 21, 22]. First, we will carry out an analysis similar to the ρ/a-scalings of the confinement time so common in plasma transport literature (ρ is the ion Larmor radius and a the minor radius of the device). The equivalent analysis in the case of the sandpile is to study how τ_E changes when the number of cells L is increased. However, it is necessary to ensure that the critical gradients and the total power remain unchanged. Therefore, if we apply the transformation $L \to \alpha L$, the following parameter transformations must be applied simultaneously:

$$(Z_c, N_F) \to \left(\frac{Z_c}{\alpha}, \frac{N_F}{\alpha}\right), \quad \left(Z_c^M, N_F^M\right) \to \left(\frac{Z_c^M}{\alpha}, \frac{N_F^M}{\alpha}\right), \quad S_0 \to \frac{S_0}{\alpha}. \quad (15)$$

Applying these transformations to equations (10)–(14), it is straightforward to obtain, in the ohmic phase, $\tau_E(\alpha L) \sim \alpha^2 \tau_E(L)$. This dependence on α is characteristic of a purely diffusive process, and we will refer to it as the sandpile *gyro-Bohm scaling*, in analogy with plasma transport terminology. In contrast, for the L-mode, $\tau_E(\alpha L) \sim \alpha \tau_E(L)$, which reveals the existence of a non-diffusive transport process dominating the dynamics (the second term in equation (11), which scales as α^{-1}, is strongly subdominant). Interestingly, the results for the ELM-free H-mode reveal that the dominant term (the first) has a gyro-Bohm scaling (it scales as α^2). That is, a diffusive mechanism (the one associated with D_e, related to the suppression of turbulent transport by a sheared-flow) has taken over control of the system transport after the L–H transition. The importance of the other two terms, which both scale as α^{-1}, will depend on the sandpile parameter values used. Finally, for both the periodic and the intermittent ELMy H-modes, a non-gyro-Bohm transport scaling is obtained, since the dominant term (the first in both cases) again scales as α. The new dominant non-diffusive transport mechanism is, in this case, related to the ELMs.

A similar analysis can be done regarding the degradation of confinement with power observed in tokamaks. To do it, it

is only necessary to carry out the transformation $P_T \to \beta P_T$, where $P_T = S_0 L$ is the total external power. In this case, it is sufficient to make the transformation $S_0 \to \beta S_0$ in equations (10)–(14). It is then found that, in the L-mode and in both ELMy H-modes the dominant term scales as β^{-1}, revealing that power degradation in the diffusive sandpile is intrinsically linked to the dominance of a non-diffusive transport process. On the other hand, no power degradation is observed in the ohmic phase, while a mixed scaling is found in the ELM-free H-mode. In it, the dominant term is independent of β, but the other terms scale as β^{-3} which, depending on the sandpile parameter values, can modify the global scaling with power. (This situation can be important if the system enters into the ELMy H-mode at powers for which the first term is not still dominating the global confinement.)

Finally, we can compare the global confinement times of the ELMy H-modes and the L-mode for the same P_T. The ratio of these times is known as the H enhancement factor in the plasma transport community [21]. For the diffusive sandpile, this ratio is roughly equal to (Z_c^M/Z_c). The enhancement can be recognized more visually by comparing τ_E for the ELMy H-mode (solid line) with the extrapolation of equation (11) (dashed line) for $S_0 > S_0^{L-H}$. As a final remark, it is interesting to notice that the intermittent and the periodic H-modes have very similar global confinement properties. Not only does τ_E have a gyro-Bohm scaling in both regimes, but the values of τ_E are also within 5–10% of each other. This similarity is due to the small difference in mass stored in the SOC pedestal in the two regimes. In contrast, the dynamics of ELMs are intrinsically different.

5. Characterization of Type-I ELMs in the diffusive sandpile

We will first characterize the periodic ELM-like oscillations occuring in the periodic H-mode (i.e. for $D_e(Z_c^M - N_F/2)/L < S_0 < D_e(N_F^M)^2/\kappa_c$). Their frequency can be obtained numerically in several ways. For instance, in figure 6 the power spectra of the fluxes leaving the sandpile are shown for increasing powers. The dominant frequency (and some of its first harmonics) is clearly identified as a peak in the spectrum. In the inset of the same figure, the frequencies corresponding to these peaks are plotted against S_0, and $\nu_{PS} \sim S_0^{(1.08\pm0.01)}$ is obtained when fitting them to a power law.

A very similar number is obtained when looking instead for break points in the rescaled-range analysis (R/S) of the flux time series (see figure 7). The R/S analysis is a well-known method to look for temporal correlations in a time series [23]. For a time series of length N, we form ordered subsets of length $n \leqslant N$: $X = X_k, k = 1, 2, \ldots, n$, with mean $\bar{X}_n$ and variance S_n^2. Then, we define:

$$\left(\frac{R}{S}\right)_n = \frac{\max(0, W_1, \ldots, W_n) - \min(0, W_1, \ldots, W_n)}{\sqrt{S_n^2}}, \tag{16}$$

where $W_k = X_1 + \cdots + X_k - k\bar{X}_n$. Hurst showed that for self-similar signals, $R/S \sim n^H$ for some ranges of time lags n. H is known as the Hurst exponent, and is equal to 0.5 for a random signal, while $H > 0.5$ implies correlation and $H < 0.5$ anticorrelation. When any periodicity is present in the signal,

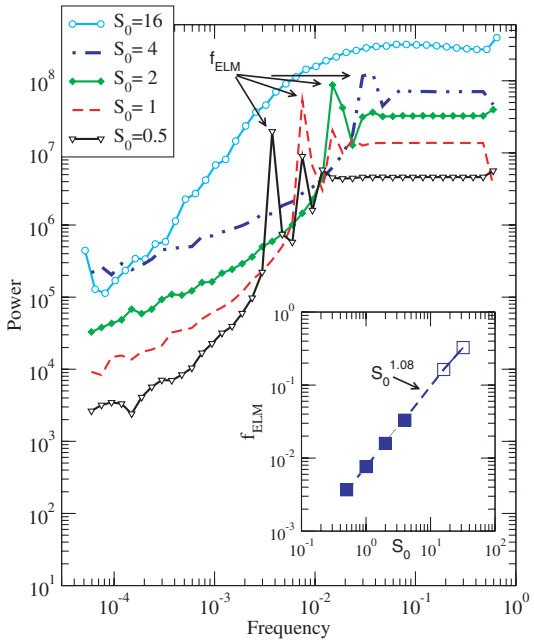

Figure 6. Power spectra of the fluxes leaving the sandpile in the ELMy H-mode regime for increasing S_0. Inset: scaling of the mean ELMing frequency with S_0; full squares correspond to the periodic H-mode, and open squares to the intermittent H-mode.

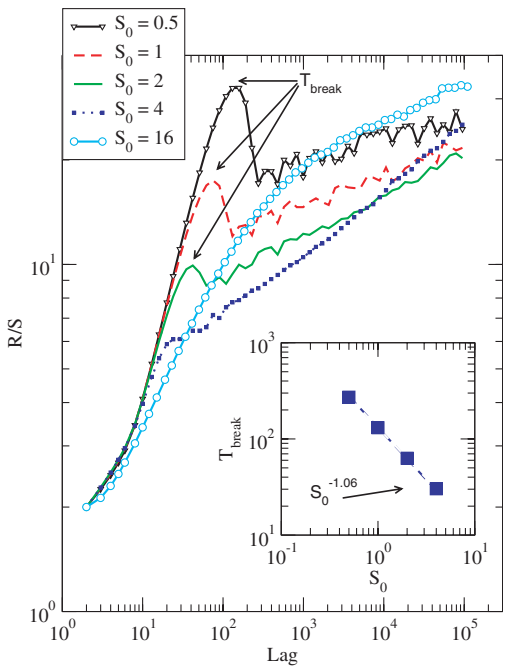

Figure 7. R/S analysis of the fluxes leaving the sandpile in the ELMy H-mode regime for increasing S_0. Inset: scaling of T_{break} with S_0.

the R/S trace exhibits an abrupt break point for n equal to the signal period. At n smaller than the break point a region with $H \sim 1$ exists, while a much flatter region with $H \sim 0$ is found slightly above [8]. In the case of our flux series, $\nu_{R/S} = T_{break}^{-1} \simeq S_0^{1.06\pm0.02}$ (see inset), which coincides with the characteristic frequency found in the power spectrum.

Another analytical tool of interest to detect periodic and intermittent behaviour in a time signal is the shape of the

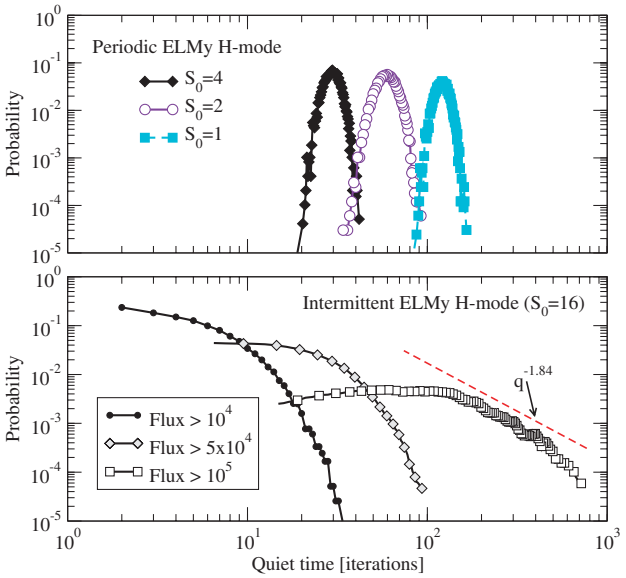

Figure 8. Probability density function (pdf) of the quiet times between ELMy relaxations in the periodic (above) and intermittent (below) H-modes. In the intermittent case, several pdfs for the same power ($S_0 = 16$) have been computed, in which only those ELMs associated with a flux larger than some prescribed threshold are considered. As the threshold value increases, the pdf develops power laws characteristic of SOC as shown in [24].

probability density functions (pdf) of the quiet times between events. The basics of this technique were first explored in the context of the sandpile [24], but they have proved to be useful when analysing experimental data as well [9]. In figure 8, we construct this pdf for the sandpile outflux time series. The result is a very peaked function centred at $q \simeq T_{\rm break}$, as should be expected from a series of quasi-periodic events.

The numerical finding of such strong periodicity is somewhat unexpected. The access to the second critical gradient at powers not sufficiently large as to overdrive the system should yield scale-free SOC transport, not quasi-periodic relaxations. The cause for this strong periodicity must be looked for in the large value of $D_{\rm e}(N_{\rm F}^{\rm M})^2/S_0 > \kappa_{\rm c}$, due to the large value of $N_{\rm F}^{\rm M}$ associated with the ideal mode. This forces the SOC pedestal to stay in the quasi-periodic regime already encountered in the simple diffusive sandpile at values of $\kappa > \kappa_{\rm c}$ [16]. Therefore, the dynamics dominating the SOC pedestal transport in the periodic ELMy H-mode are no longer critical. Instead, transport takes place through periodic relaxations which are triggered at the sandpile edge with periodicity $\nu \simeq S_0/N_{\rm F}^{\rm M}$. Two characteristic signatures of this dynamical regime [16] are indeed observed numerically, confirming this conclusion: (1) the linear slope profile with absolute value varying between $Z_{\rm c} - N_{\rm F}^{\rm M}/2$ and $Z_{\rm c}$ across the SOC pedestal region (see profile in full squares in figure 2), and (2) a strong peaking at the sandpile edge of the pdf of the locations at which avalanches are triggered.

For larger powers, κ can get sufficiently small to make the SOC pedestal change into a SOC regime. Then the pedestal discharges through intermittent scale-free avalanches. The average frequency of these events still scales linearly with S_0 (see figure 6), but all characteristic features of critical SOC dynamics are recovered. For instance, the peaks in the power spectrum and the breaking point in the R/S curve vanish (see figures 6 and 7). In the same way, the quiet time pdf (see figure 8) recovers the exponential shape characteristic of a randomly driven system, and reveals the existence of SOC dynamics upon the use of intensity thresholding of the ELM events in the fashion proposed in [24]. In the same way, the slope across the SOC pedestal becomes constant (roughly $Z \simeq -(Z_{\rm c}^{\rm M} - N_{\rm F}^{\rm M}/2)$), and the pdf of avalanche initiation locations becomes much wider and peaked at the inner part of the SOC pedestal. All these features are characteristic of the SOC regime, as previously observed in the simple diffusive sandpile [16].

6. Conclusions

In this paper we have shown that the SOC paradigm for plasma turbulent transport in the L-mode can be extended, in a physically meaningful way for confined plasmas, by introducing new dynamics that allow a transition to enhanced confinement modes. The physical mechanisms added include the suppression of local transport induced by a turbulence-generated shear-flow, some kind of diffusive transport and the existence of a second critical gradient that is larger than the one dominating the dynamics in the L-mode. This can be done by including a handful of new free parameters and evolution rules. When these elements are implemented in a simple sandpile model, the resulting system exhibits, in spite of its simplicity, many of the characteristic features of enhanced confinement modes in plasmas. Specifically, these features include an improvement of global confinement, a transition from non-gyro-Bohm to gyro-Bohm scaling in the confinement time, the formation of an edge pedestal and the excitation of strongly periodic Type-I ELM-like activity.

All of these results seem to suggest that much of the phenomenology observed in enhanced modes in plasmas might not depend too strongly on the details of the unstable modes involved but instead on the character of their associated transport. For instance, knowledge of the details of the linear growth and non-linear saturation phases of the resistive and/or ideal modes that might be related to the two critical gradients may be less important than knowledge of whether the dynamics are avalanche-like or diffusive, memoryless or critical, or scale-free or single-scale dominated. In a way, the sandpile model suggests that the system tries to balance the external power with all means at its disposal and that the changes in dynamics respond to the need to transport larger and larger fluxes out of the system. It also suggests some interesting ideas that might guide the study of edge phenomena with more sophisticated models/codes. For instance, the local power balance between diffusive and/or avalanche transport channels might be ultimately responsible for setting the pedestal width. Similarly, this model confirms that a very essential role might be played by the interaction between diffusive and avalanche transport, as previously suggested in [11]. This might be of special relevance at the edge region in order to obtain periodic ELMing. This hypothesis might perhaps be tested by looking for increasing ELM intermittency in tokamaks at higher powers, even when the required powers might not be attainable without encountering a disruption.

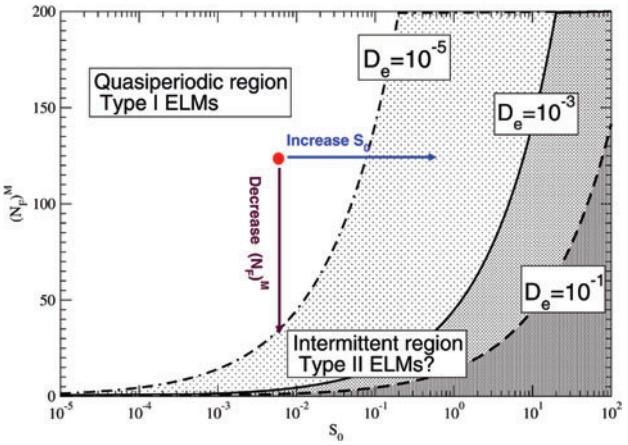

Figure 9. Sketch of the periodic–intermittent transition. From an arbitrary point (○) in the periodic ELMy region, the transition curve (shown by dashed/full lines for three different values of the diffusivity D_e) can be crossed by either increasing the power S_0 or by decreasing $(N_F)^M$.

Another interesting idea suggested by our studies stems from a different interpretation of the periodic–intermittent ELM transition. As we mentioned before, the transition point is crossed as the external power is increased (see figure 9). However, the fact that the transition point depends solely on $\kappa = D_e(N_F^M)^2/S_0$ implies that an analogous transition from quasi-periodic to intermittent relaxations would also take place as N_F^M is reduced, even at constant power. However, the intermittent relaxations would now be considerably smaller and of higher frequency, which would allow quieter disposal of the incoming power. This situation is somewhat reminiscent of the excitation of Type-II ELMs observed in experiments when the stability properties of the discharges are improved. In fact, N_F^M is nothing other than a coarse measure of the strength of the local instability. Finally, it is worth mentioning that, as it is, our diffusive sandpile model does not exhibit anything similar to Type-III ELMs. However, preliminary work suggests that, by adding some details of the interaction between local fluctuations and sheared flows, small edge relaxation oscillations with frequencies that decrease with increasing power might be obtained at the onset of the L–H transition (more precisely, in the range of powers $N_F/2 + D_0Z_c \leqslant S_0L \leqslant N_F + D_0Z_c$). These results would then suggest that the appearance of Type-III ELMs in a confined plasma might be related to the dynamics of the formation of the edge transport barrier at the onset of the L–H transition.

Acknowledgments

Valuable discussions with M. Varela, U. Bhatt, B.Ph. van Milligen and A. Loarte are acknowledged. Research supported in part by Spanish DGES Proyects Nos FTN2000-0965 and FTN2000-0924-C03-01 and by the Office of Fusion Energy, US DOE, under contracts DE-AC05-00OR22725 and DE-FG03-99 ER54551.

References

[1] Bak P., Tang C. and Weisenfeld K. 1987 *Phys. Rev. Lett.* **59** 381
[2] Diamond P.H. and Hahm T.S. 1995 *Phys. Plasmas* **2** 3640
[3] Newman D.E., Carreras B.A., Diamond P.H. and Hahm T.S. 1996 *Phys. Plasmas* **3** 1858
[4] Wesson J. 1988 *Tokamaks* (Cambridge: Cambridge University Press)
[5] Lopez-Cardoso N. 1995 *Plasma Phys. Control. Fusion* **37** 799
[6] Carreras B.A. *et al* 1999 *Phys. Rev. Lett.* **83** 3653
[7] Pedrosa M.A. *et al* 1999 *Phys. Rev. Lett.* **82** 3621
[8] Carreras B.A. *et al* 1998 *Phys. Rev. Lett.* **80** 4438
[9] Sanchez R., Van Milligen B.Ph., Newman D.E. and Carreras B.A. 2003 *Phys. Rev. Lett.* **90** 185005
[10] Politzer P.A. 2000 *Phys. Rev. Lett.* **84** 1192
[11] Sanchez R., Newman D.E. and Carreras B.A. 2001 *Nucl. Fusion* **41** 247
[12] Chapman S.C., Dendy R.O. and Hnat B. 2001 *Phys. Rev. Lett.* **86** 2814
[13] Hicks H.R. and Carreras B.A. 2001 *Phys. Plasmas* **8** 3277
[14] Diamond P.H., Liang Y.-M., Carreras B.A. and Terry P.W. 1994 *Phys. Rev. Lett.* **72** 2565
[15] Connor J.W. and Wilson H.R. 2000 *Plasma Phys. Control. Fusion* **42** R1
[16] Newman D.E., Sanchez R., Carreras B.A. and Ferenbaugh W. 2002 *Phys. Rev. Lett.* **88** 204304
[17] Wagner F. *et al* 1982 *Phys. Rev. Lett.* **49** 1408
[18] Petty C.C. *et al* 1995 *Phys. Plasmas* **2** 2342
[19] Zohm H. 1996 *Plasma Phys. Control. Fusion* **38** 105
[20] Gruzinov I., Diamond P.H. and Rosenbluth M.N. 2002 *Phys. Rev. Lett.* **89** 255001
[21] Carreras B.A. 1992 *IEEE Trans. Plasma Sci.* **25** 1281
[22] Stroh U. 1998 *Plasma Phys. Control. Fusion* **40** 9
[23] Hurst H.E. 1951 *Trans. Am. Soc. Civ. Eng.* **116** 770
[24] Sanchez R., Newman D.E. and Carreras B.A. 2002 *Phys. Rev. Lett.* **88** 068302